

Quantum-Enhanced Tunable Second-Order Optical Nonlinearity in Bilayer Graphene

Sanfeng Wu¹, Li Mao², Aaron M. Jones¹, Wang Yao³, Chuanwei Zhang², Xiaodong Xu^{1,4,*}

¹ Department of Physics, University of Washington, Seattle, Washington 98195, USA

² Department of Physics and Astronomy, Washington State University, Pullman, Washington, 99164 USA

³ Department of Physics and Center of Theoretical and Computational Physics, The University of Hong Kong, Hong Kong, China

⁴ Department of Material Science and Engineering, University of Washington, Seattle, Washington 98195, USA

Abstract

Second order optical nonlinear processes involve the coherent mixing of two electromagnetic waves to generate a new optical frequency, which plays a central role in a variety of applications, such as ultrafast laser systems, rectifiers, modulators, and optical imaging. However, progress is limited in the mid-infrared (MIR) region due to the lack of suitable nonlinear materials. It is desirable to develop a robust system with a strong, electrically tunable second order optical nonlinearity. Here we demonstrate theoretically that AB-stacked bilayer graphene (BLG) can exhibit a giant and tunable second order nonlinear susceptibility $\chi^{(2)}$ once an in-plane electric field is applied. $\chi^{(2)}$ can be electrically tuned from 0 to $\sim 10^5 \text{ pm/V}$, three orders of magnitude larger than the widely used nonlinear crystal AgGaSe₂. We show that the unusually large $\chi^{(2)}$ arises from two different quantum enhanced two-photon processes thanks to the unique electronic spectrum of BLG. The tunable electronic bandgap of BLG adds additional tunability on the resonance of $\chi^{(2)}$, which corresponds to a tunable wavelength ranging from $\sim 2.6 \mu\text{m}$ to $\sim 3.1 \mu\text{m}$ for the up-converted photon. Combined with the high electron mobility and optical transparency of the atomically thin BLG, our scheme suggests a new regime of nonlinear photonics based on BLG.

Keywords: bilayer graphene, second harmonic generation, double resonance enhancement, density of state, tunability, polarization

Text

Graphene-based photonics and optoelectronics^{1,2} have drawn intense interest because of their combination of unique electronic properties³, such as high electron mobility⁴ and long mean free path⁵, as well as their excellent optical properties^{1,2,6,7}, such as broadband optical absorption^{2,6,7} and ultrafast optical response^{8,9,10}. In this context, BLG may have better potential than single layer graphene for photonic applications due to its four-band electronic structure and widely tunable bandgap in the MIR¹¹. One promising application is to achieve chip-scale and electrically tunable nonlinear optical devices. Conventional nonlinear optical devices are based on bulk crystals which have poor compatibility with

integrated circuits and lack electrical tunability in intensity and wavelength. The required phase matching conditions also lead to volatile signals subject to perturbations from the environment. All these limitations prevent the integration of nonlinear photonics and advanced electronics for new photonic and optoelectronic applications. Here we show that, under realistic device conditions, the difficulties mentioned above can be overcome using the nonlinear optical properties of BLG. Therefore BLG emerges as an excellent $\chi^{(2)}$ material and may provide opportunities for new optoelectronic and photonic applications.

Figures 1a and 1b show the atomic structure of BLG and a typical dual-gate field effect transistor (FET) device¹², respectively. We calculate the intensity of SHG following a quantum description of nonlinear optical conductivity. The applied potential bias between top and bottom gates tunes the electronic properties of BLG. The Hamiltonian of BLG near the Dirac points (\mathbf{K} and \mathbf{K}') can be written as³

$$H = \sum \psi_{\mathbf{k}}^\dagger \mathcal{H}_{\mathbf{k}} \psi_{\mathbf{k}}, \quad (1)$$

where

$$\psi_{\mathbf{k}}^\dagger = (b_{\mathbf{k}}^{1\dagger}, a_{\mathbf{k}}^{1\dagger}, a_{\mathbf{k}}^{2\dagger}, b_{\mathbf{k}}^{2\dagger}),$$

and

$$\mathcal{H}_{\mathbf{k}} = \begin{pmatrix} -\Delta & \hbar v_f g & 0 & 0 \\ \hbar v_f g^* & -\Delta & \gamma_1 & 0 \\ 0 & \gamma_1 & \Delta & \hbar v_f g \\ 0 & 0 & \hbar v_f g^* & \Delta \end{pmatrix}.$$

$a_{\mathbf{k}}^{i\dagger} (b_{\mathbf{k}}^{i\dagger})$ is the creation operator for electrons at the sublattice A (B), in the layer $i (i = 1, 2)$, and with momentum \mathbf{k} in the BZ. $\mathbf{k} = (k_x, k_y)$ is the continuous wave vector from \mathbf{K}, \mathbf{K}' and $g = k_x - \xi i k_y$ is a complex number ($\xi = +1$ for \mathbf{K} and $\xi = -1$ for \mathbf{K}'). The spatial coordinates are defined in Fig. 1a and 1b. $v_f \approx 10^6$ m/s is the Fermi velocity of single layer graphene. Δ ($-\Delta$) describes the potential effect induced by the gate voltages. $\gamma_1 \approx 0.4$ eV is the inter-layer hopping parameter³. Here we ignore other hopping processes due to their relatively weak strengths. The Hamiltonian (1) has four energy bands, which are obtained by diagonalizing $\mathcal{H}_{\mathbf{k}}$, and plotted in Figure 1c for $\Delta = 0$.

The total Hamiltonian $\mathcal{H}_{\mathbf{p}}$ that includes the interactions between the BLG and normal incident MIR photons can be obtained by replacing the momentum vector $\hbar\mathbf{k}$ in $\mathcal{H}_{\mathbf{k}}$ with $\mathbf{p} = \hbar\mathbf{k} + e\mathbf{A}$, where \mathbf{A} is the vector potential of the optical fields^{3,13,14,15}. The evolution of the electronic state is determined by the quantum Liouville equation¹⁶:

$$i\hbar\partial_t \rho = [\mathcal{H}_{\mathbf{p}}, \rho] - i\Gamma(\rho - \rho_{t=0}), \quad (2)$$

where ρ is the time dependent quantum state of electrons with momentum \mathbf{k} at temperature T and chemical potential μ . Γ is a phenomenological parameter for describing the relaxation of electronic states. We set $\Gamma = 0.05$ eV in our calculations¹⁷, which corresponds to ~ 80 fs relaxation time of electrons. This is a conservative estimation even at room temperature (The effect of Γ is discussed in supplemental materials¹⁸). The steady state density matrix in the presence of the optical fields can be obtained by solving the time-dependent equation (2) perturbatively¹⁶ (see supplemental materials¹⁸).

The optically induced electric current is defined as^{19,20,21}

$$j_s = ve \sum_{BZ} \text{tr}(\rho \frac{\partial \mathcal{H}_p}{\partial \mathbf{p}}) = \sigma_1 \mathbf{E} e^{i\omega t} + \sigma_2 E^2 e^{i2\omega t} + c.c + \dots, \quad (3)$$

where $v = 2$ describes the spin degeneracy and \mathbf{E} is the electric field. σ_1 is the linear optical conductivity, which value obtained from our approach is exactly the same as the ones reported using the Kubo formula⁷. Here we focus on the second order nonlinear optical conductivity σ_2 , which is responsible for SHG. The simplified formula of σ_2^α is¹⁸:

$$\sigma_2^\alpha = \frac{e}{2\pi^2 E^2} \int_{BZ} \sum_{ijkl} \left[\frac{\rho_k^{ii} - \rho_k^{ll}}{\hbar\omega + \epsilon_i - \epsilon_l - i\Gamma} - \frac{\rho_k^{ll} - \rho_k^{jj}}{\hbar\omega + \epsilon_l - \epsilon_j - i\Gamma} \right] \frac{(H_{\text{int}})_{il} (H_{\text{int}})_{lj} (\eta^\alpha)_{ji}}{2\hbar\omega + \epsilon_i - \epsilon_j - i\Gamma} d\mathbf{k}, \quad (4)$$

where $\alpha = x, y$; $\eta^\alpha = \frac{\partial \mathcal{H}_p}{\partial p_\alpha}$; $H_{\text{int}} = \mathcal{H}_p - \mathcal{H}_k$ is the interaction Hamiltonian and $\rho_k = \text{diag}[f_1, f_2, f_3, f_4]$ is the initial state obtained from the Fermi-Dirac distribution $f_i = \frac{1}{\exp[(\epsilon_i - \mu)/k_B T] + 1}$ of electrons at different bands with the band energy ϵ_i ($i = 1, 2, 3, 4$). μ is the chemical potential, k_B is the Boltzmann constant, and T is the temperature.

The above equation (4) has a trivial solution $\sigma_2^\alpha = 0$, although the inversion symmetry of intrinsic BLG (C_{3v} group) has been broken by the vertical biased potential. This is due to the cancellation of the optically-excited second order electrical current at opposite momenta ($+\mathbf{k}$ and $-\mathbf{k}$) with respect to both Dirac points. In order to generate a non-zero second order optical nonlinearity, we introduce an in-plane electrical current between source and drain to suppress the cancellation. From semi-classical electron transport theory, the in-plane electric field shifts the Fermi surface by $\Delta\mathbf{k} = \frac{m^* u_m j_{\text{sc}}}{\hbar \sigma_{\text{dc}}}$, where m^* is the electronic effective mass, j_{sc} is the in-plane current density, σ_{dc} is the DC conductivity, and u_m is the mobility¹⁸ (Fig. 1c). According to experimental data of BLG^{1,2,22,23}, we take $m^* \approx 0.05m_e$, $u_m \approx 1 \frac{m^2}{Vs}$, $\sigma_{\text{dc}} \approx \frac{e^2}{h}$. An energy shift of $\hbar v_f |\Delta\mathbf{k}| \approx 0.01 \text{ eV}$ is achievable with a DC current $j_{\text{sc}} \approx 8 \text{ nA/nm}$. As a result, the Fermi level is shifted (Fig. 1c) and the initial electronic state in the presence of j_{sc} turns out to be $\rho_k \leftarrow \rho_{k-\Delta\mathbf{k}}$. Physically, due to the Pauli exclusion principle, part of the optical transitions are blocked due to the Fermi level shifting. Therefore the $+\mathbf{k}/-\mathbf{k}$ symmetry is broken and SHG becomes nonzero.

We first explore the second order nonlinear optical conductivity with circularly polarized light excitations. For simplicity, we use left circular polarization as an example. Figures 2a and 2b plot both the real and imaginary parts of the second order optical conductivity σ_2 at temperatures 30 K and 300 K, respectively. σ_2 is decomposed into x and y directions. The induced current at twice the optical frequency has a strong phase-correlation between the x and y directions: $\sigma_2^y = -i\sigma_2^x$. It therefore implies the left circular polarization of the new optical fields generated by SHG are the same as the incident beam. We set the chemical potential $\mu = \gamma_1/2 = 0.2 \text{ eV}$ without the bandgap opening (i.e., $\Delta = 0$). The in-plane electric field is along the y direction, leading to a shift of $\hbar v_f |\Delta\mathbf{k}| \sim 0.01 \text{ eV}$. A surprising finding here is the giant enhancement of σ_2 at $\omega = 0.2 \text{ eV}$ and 0.4 eV , as seen from the resonant peaks in Figures 2a and 2b. The intensities of the resonant peaks increase as the temperature decreases. The ratio of σ_2 at low temperature (30K) to high temperature (300K) is about 1.5. In Fig. 2c, we plot σ_2 as a function of both temperature and frequency, where these features can be clearly seen.

The two resonant peaks arise from different quantum-enhancement mechanisms. At

$\omega = 0.4 \text{ eV}$ the optical process is dominated by the transitions from the 2nd to the 4th band (Fig. 2d) through two-photon absorption. Although two-photon absorption can happen even in BLG in equilibrium^{24,25}, the contributions to SHG from the $\mathbf{K} + \mathbf{k}$ and $\mathbf{K} - \mathbf{k}$ points cancel out. As we mentioned above, the in-plane electric field breaks this symmetry, leading to a shift of the Fermi surface to avoid such cancellation. More importantly, when $\omega = \Delta E_{23} = \Delta E_{34}$ (ΔE_{ij} is the energy difference between the bands i and j), the transient state of SHG is a real state (i.e. the electronic state in the 3rd band), giving rise to resonantly enhanced contribution as compared to conventional SHG where the intermediate states are virtual states. In this case, the so-called double resonance enhanced (DRE) harmonic generation happens in the BLG system. The signal intensity of DRE SHG²⁶ is usually proportional to $1/\Gamma^2$.

At $\omega = 0.2 \text{ eV}$, the high joint density-of-states (HJDOS) come into play. As we see from Figure 2d, the energy splitting $\Delta E_{34} \approx \gamma_1$ is nearly a constant for a large range of \mathbf{k} , which allows plenty of resonant 2-photon transitions when the incident laser frequency $\omega \sim \frac{\gamma_1}{2} = 0.2 \text{ eV}$, giving rise to a significant enhancement of SHG. Clearly, the enhancement of SHG at both $\omega = 0.4 \text{ eV}$ and 0.2 eV originates from the special band structure of the BLG.

We now explore the second order nonlinear optical conductivity with linearly polarized light excitations. Figure 3 shows σ_2 at the two quantum-enhanced resonant peaks ($\omega = 0.2 \text{ eV}$ and 0.4 eV) as a function of the incident polarization angle φ with respect to the x -axis. The temperature is set at 180K. The red solid line denotes the nonlinear response along the x direction, with the blue dashed line along the y direction. We note that the induced current in the two directions have almost the same phase, which indicates that the output SHG is still linearly polarized. When we vary the incident angle, the optical conductivities at two different resonant frequencies behave differently. (1) σ_2 enhanced by HJDOS has a polarization angle $2\varphi + \frac{\pi}{2}$ (Fig. 3a). For instance, when the incident laser is polarized at $\varphi = \frac{\pi}{4}$, the second order nonlinear optical conductivity is polarized with angle π , i.e. in the x direction. (2) The optical current excited by the DRE mechanism has a preferred axis (y -axis) (Fig. 3b). The signal generated in the y direction (where the in-plane electric field lies) is larger than that in the x direction. Therefore the output SHG intensity in this situation oscillates around the y -axis as φ varies.

Here we note that the symmetric patterns in Fig. 3 do not depend on the relative direction of the in-plane electric fields and lattice orientation. For simplicity, we here set the applied bias along the lattice direction ($-y$), which is not necessary in practice. In general, we find that the second order optical response always behaves in the same way as that shown in Fig. 3 for varying directions of the DC current, which determines the symmetric axis of the polar plots (supplementary materials).

The second order optical susceptibility $\chi^{(2)}$ can be estimated from the optical conductivity¹⁹:

$$\chi^{(2)} = \frac{\sigma_2}{\omega \epsilon_0 d_{\text{BLG}}}. \quad (5)$$

Here $d_{\text{BLG}} \sim 0.66 \text{ nm}$ is the thickness of BLG and $\epsilon_0 = 8.85 \times 10^{-12} \text{ C/Vm}$ is the vacuum permittivity. Using ev_f/V^2 as a unit for σ_2 , we have $\chi^{(2)} \sim 10^5 \text{ pm/V}$, about three orders of magnitude larger than state-of-the-art nonlinear crystals in MIR. For comparison, the second order nonlinear susceptibility of the widely used AgGaSe₂ crystal

is **68 pm/V** at a wavelength of $\sim 2.1 \mu\text{m}$ ²⁷. At low temperature and with a large in-plane electric field, the value can be even larger and the response region in our scheme is ultra-broad, as shown below.

We now show that the giant SHG can be tuned by the in-plane electric field, Fermi level, and biased potential Δ . Fig. 4a plots the nonlinear optical conductivity at two resonant peaks as a function of the in-plane current, which is estimated from the shift of the Fermi surface (Δk). As an example, the incident laser is set to be polarized in the x direction and j_{sc} is in the y direction at a temperature of 180 K. The Fermi level is set to be **0.2 eV**. The red stars in the figure represent the parameters we used in the previous discussions in this paper. This plot indicates that SHG intensity increases linearly when the in-plane current is small ($< \sim 35 \text{ nA/nm}$), and saturates at high in-plane current. Apparently, if we turn off the in-plane field, SHG is consequently switched off. Unlike conventional electric field-induced SHG which requires an extremely large electric voltage²⁸ (kilovolts) in the crystal, small in-plane electric fields are more favorable in device applications. In BLG, with an electric field of $\sim 1 \text{ V/mm}$, one can electrically switch on and off SHG.

The SHG signal can also be tuned by adjusting the Fermi level, as shown in Fig. 4b. Obviously, there is a pronounced SHG when the Fermi level falls in the range around $\frac{E_1}{2} = \mathbf{0.2 eV}$ with $\Delta = 0$. If we increase or decrease the Fermi level without crossing the Dirac point, the effects of the DRE and HJDOS become less important and the signal decreases to zero. One may notice that the SHG signal will recover when the Fermi level goes down to -0.2 eV (in the p-doping situation).

Finally, we show that the unique bandgap tunability of BLG by an interlayer bias induces the widely tunable resonant frequency of SHG. The intensity plot in Fig. 4c shows the magnitude of the second order optical conductivity as a function of Δ and incident laser frequency. In addition to the change of the amplitude of σ_2 , an important effect is the variation of the resonant frequency ω_0 , indicated in Fig. 4c by the dashed lines. ω_0 increases from 0.4 to $\sim 0.48 \text{ eV}$ for the DRE peak and from 0.2 eV to $\sim 0.25 \text{ eV}$ for the HJDOS peak, as Δ is tuned from 0 to 0.15 eV. Therefore the resonant wavelengths for SHG are electrically tunable from $\sim 5 \mu\text{m}$ to $\sim 6 \mu\text{m}$ and from $\sim 2.6 \mu\text{m}$ to $\sim 3.1 \mu\text{m}$. This is another remarkable advantage as compared to conventional nonlinear crystals, where the wavelength for SHG can only be changed by rotating the crystal angles. Moreover, due to its atomic thickness, BLG requires no phase matching condition, which is crucial in conventional SHG. Phase matching usually leads to increased sensitivity to environmental perturbations, such as temperature. Therefore, from this point of view, SHG of BLG is robust.

In conclusion, we propose a new scheme based on BLG as a nonlinear optical material, with an extremely large second order optical susceptibility $\chi^{(2)} \sim 10^5 \text{ pm/V}$. We find that this enhancement arises from two different types of quantum-enhanced mechanisms, unique to the electronic structure of BLG. Our calculation shows an excellent electrical tunability of the optical nonlinearity in both intensity and wavelength compared to conventional nonlinear crystals. Considering graphene's many unique properties, we believe that our results encourage further experimental investigation towards nonlinear photonics based on BLG and may open new opportunities for graphene applications.

Corresponding Author

*Email: xuxd@uw.edu

Acknowledgements:

This work is supported by DARPA YFA N66001-11-1-4124. L. Mao and C. Zhang are supported by DARPA-YFA N66001-10-1-4025, DARPA-MTO (FA9550-10-1-0497), and NSF-PHY (1104546). A. Jones is supported by NSF Grant No. DGE-0718124. W. Yao is supported by Research Grant Council of Hong Kong.

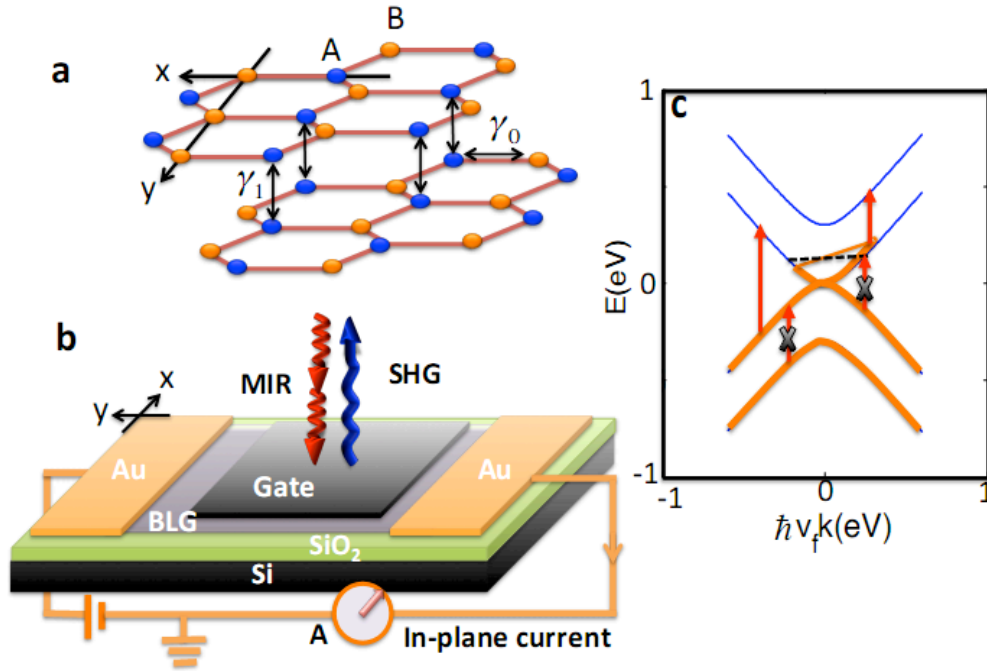


Figure 1. Dual-gated bilayer graphene FET and its optical transitions. (a) Atomic structure of AB-stacked bilayer graphene. γ_1 and γ_0 are the inter- and intra- layer hopping parameters. The coordinates used in the calculations are shown. (b) Experimental schematic of using a dual-gated bilayer graphene FET to realize SHG. The in-plane current is set in the $-y$ direction in our calculation. (c) Energy spectrum of BLG and Fermi level shifting when there is an in-plane current between source and drain. Possible and forbidden optical transitions are shown as red arrows. Brown color on the energy levels denotes the occupied states.

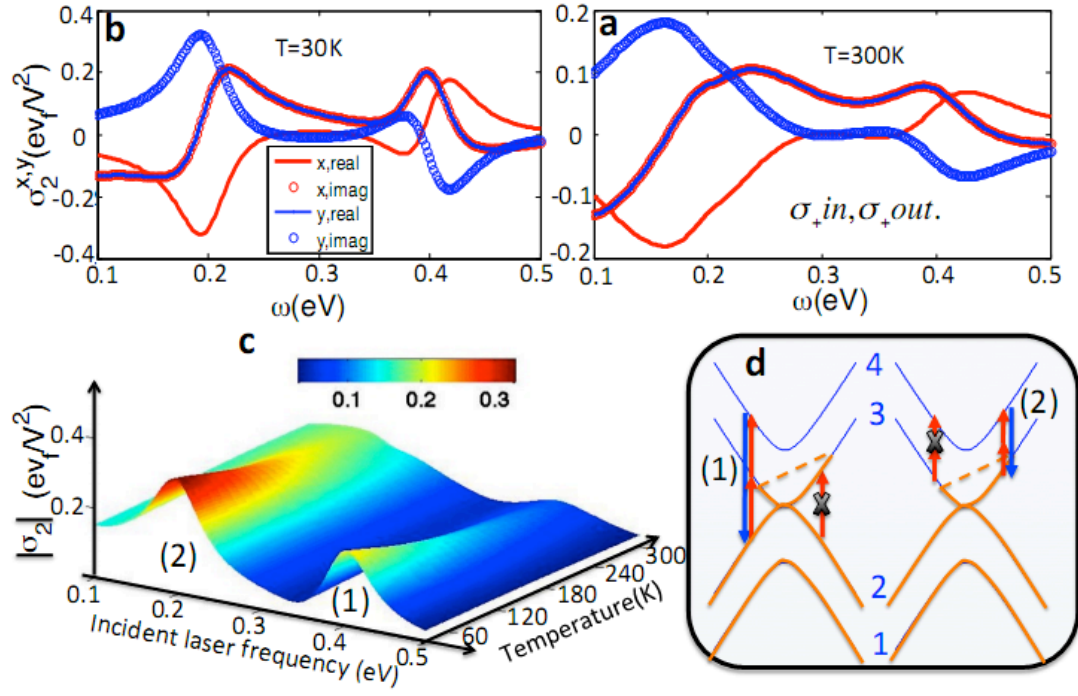


Figure 2. Second order optical response of BLG under left-hand circularly polarized incident laser beam. (a) and (b), frequency dependent nonlinear optical conductivity σ_2 calculated at a temperature of 30K and 300K, respectively. The interlayer hopping parameter $\gamma_1 = 0.4 \text{ eV}$ and the phenomenal energy broadening Γ is set to 0.05 eV . Both real and imaginary parts are shown on both x and y directions. The plots show that there are strongly enhanced responses located at $\omega = 0.2 \text{ eV}$ and 0.4 eV . (c) σ_2 as a function of temperature and laser frequency. (d) Corresponding optical process for the response peak at (1) $\omega = 0.4 \text{ eV}$ and (2) 0.2 eV .

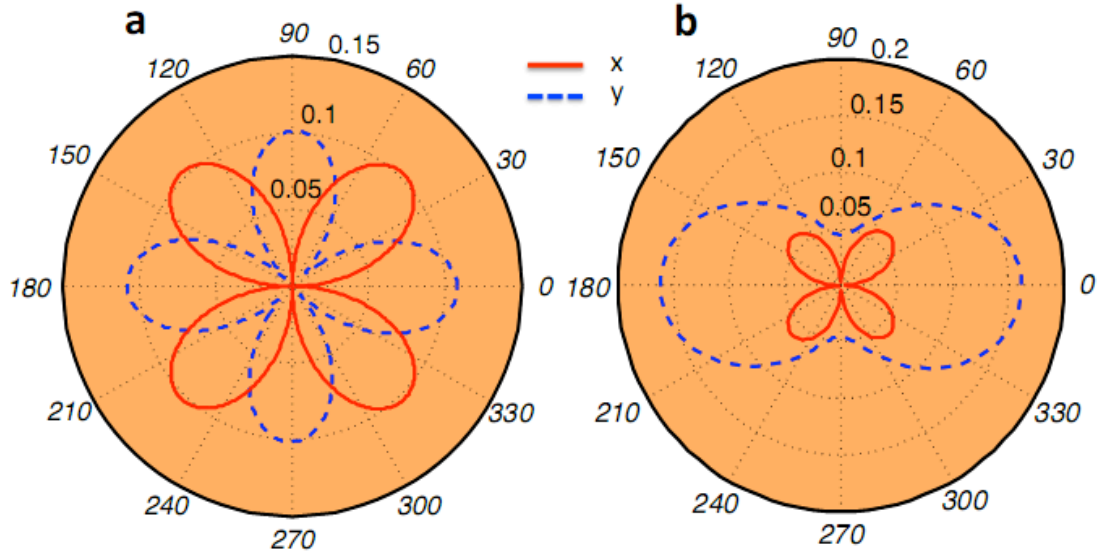


Figure 3. Second order optical response of BLG under linearly polarized incident laser beam. Polar plots of σ_2 versus varying polarization angles of the incident beam starting from the x -axis at $T=180$ K for (a), $\omega = 0.2$ eV and (b), $\omega = 0.4$ eV. The red solid and blue dashed curves correspond to the response in the x and y directions, respectively.

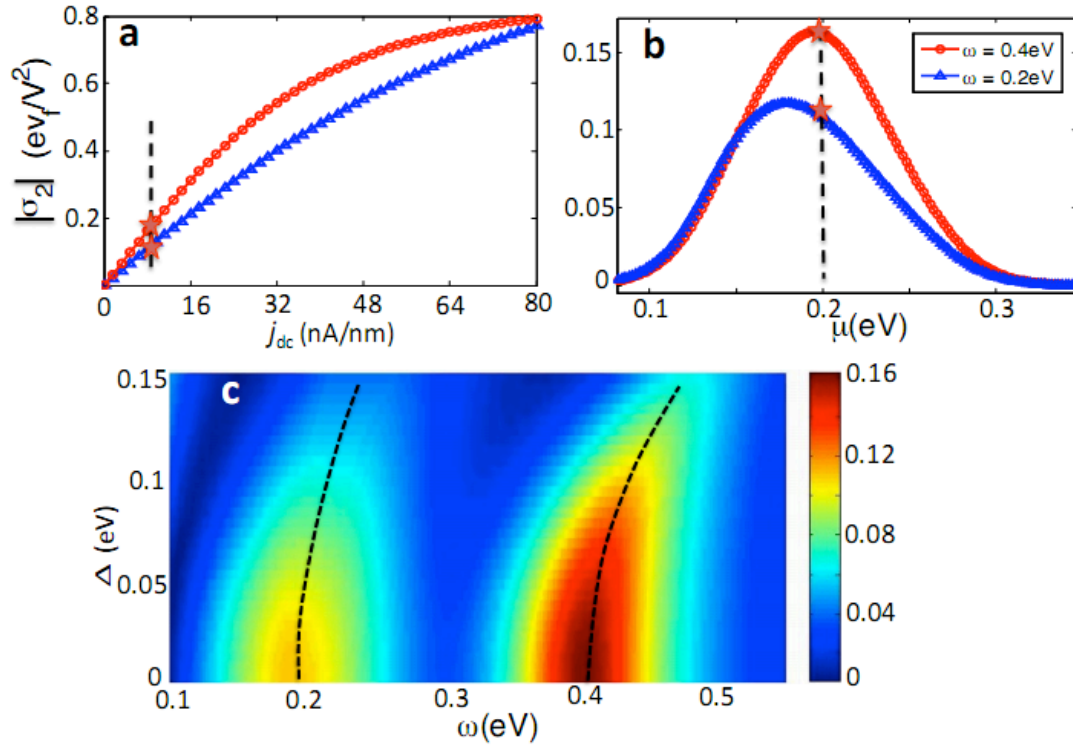


Figure 4. Tunable effects of SHG of BLG. (a) Amplitude of σ_2 as a function of estimated in-plane current ($\mu = 0.2 \text{ eV}$). (b) Amplitude of σ_2 as a function of Fermi level μ . The red star denotes the value used in our previous calculations. (c) Tunable SHG by controlling the electronic bandgap of BLG. The black dashed lines denote the resonant frequencies. Temperature is set to 180 K.

Reference:

- (1) Geim, A. K. & Novoselov, K. S., The rise of graphene. *Nature Mater.* **6** 183-191 (2007).
- (2) Bonaccorso, F., Sun, Z., Hasan, T. & Ferrari, A. C. Graphene photonics and optoelectronics. *Nature Photon.* **4**, 611-622 (2010).
- (3) Neto, A. H. C., *et al.*, The electronic properties of graphene, *Rev. Mod. Phys.* **81**, 109 (2009).
- (4) Bolotin, K. I. *et al.* Ultrahigh electron mobility in suspended graphene. *Solid State Commun.* **146**, 351-355 (2008).
- (5) Du, X., Skachko, I., Barker, A. & Andrei, E. Y. Approaching ballistic transport in suspended graphene. *Nature Nanotech.* **3**, 491-495 (2008).
- (6) Nair, R. R. *et al.* Fine Structure Constant Defines Visual Transparency of Graphene. *Science* **320**, 1308, (2008).
- (7) Abergel, D. S. L., & Fal'ko, V. I., Optical and magneto-optical far-infrared properties of bilayer graphene. *Physical Review B* **75**, 155430 (2007)
- (8) Xia, F., Mueller, T., Lin, Y.-m., Valdes-Garcia, A. & Avouris, P. Ultrafast graphene photodetector. *Nature Nanotech.* **4**, 839-843 (2009).
- (9) Mueller, T., Xia, F. & Avouris, P. Graphene photodetectors for high-speed optical communications. *Nature Photon.* **4**, 297-301 (2010).
- (10) Sun, D., Aivazian, G., Jones, A. M., Yao, W., Cobden, D., & Xu, X., New Aspects of Photocurrent Generation at Graphene pn Junctions Revealed by Ultrafast Optical Measurements, to be published in *Nature Nanotechnology* (2012)
- (11) Zhang, Y., *et al.* Direct observation of a widely tunable bandgap in bilayer graphene, *Nature* **459**, 820-823 (2009)
- (12) Meric, I. *et al.* Current saturation in zero-bandgap, top-gated graphene field-effect transistors. *Nature Nanotech.* **3**, 654-659 (2008).
- (13) Mishchenko, E. G., Dynamic Conductivity in Graphene beyond Linear Response, *Physical Review Letter*, **103**, 246802 (2009)
- (14) Mikhailov, S. A., "Non-linear electromagnetic response of graphene" *Euro. Phys. Lett.* **79**, 27002 (2007).
- (15) Rosenstein, B., Lewkowicz, M., Kao, H.C., & Korniyenko, Y., "Ballistic transport in graphene beyond linear response," *Phys. Rev. B* **81**, 041416(R) (2010).
- (16) Landau, L. D., & Lifshitz, E. M. (1977). Quantum Mechanics, Non-Relativistic Theory: Volume 3. Oxford: Pergamon Press. pp.41. ISBN 0080178014.; Sakurai, J.J., Modern Quantum Mechanics, revised edition, by Addison-Wesley Publishing Company, Inc. 1994
- (17) Nandkishore, R., & Levitov, L., Polar Kerr Effect and Time Reversal

- Symmetry Breaking in Bilayer Graphene, *Phys. Rev. Lett.* **107**, 097402 (2011)
- (18) See supplemental materials
 - (19) Hendry, E., *et al*, Coherent Nonlinear Optical Response of Graphene, *Phys. Rev. Lett.* **105**, 097401 (2010)
 - (20) Ang, Y. S., Sultan, S., & Zhang, C., Nonlinear optical spectrum of bilayer graphene in the terahertz regime, *Appl. Phys. Lett.* **97**, 243110 (2010)
 - (21) Lewkowicz, M., & Rosenstein, B., “Dynamics of particle-hole pair creation in graphene,” *Phys. Rev. Lett.* **102**, 106802 (2009).
 - (22) Zhang L. M., *et al*, Determination of the electronic structure of bilayer graphene from infrared spectroscopy, *Phys. Rev. B* **78**, 235408 (2008)
 - (23) Zou K., *et al*, Effective mass of electrons and holes in bilayer graphene: Electron-hole asymmetry and electron-electron interaction, *Phys. Rev. B* **84**, 085408 (2011)
 - (24) Yang, H., Feng, X., Wang, Q., Huang, H., Wei Chen, W., Wee, A. T. S., & Ji, W., Giant Two-Photon Absorption in Bilayer Graphene, *Nano Lett.*, **11** (7), pp 2622–2627, (2011).
 - (25) Lim, G., Chen, Z., *et al*, Giant broadband nonlinear optical absorption response in dispersed graphene single sheets, *Nature Photonics* **5**, 554–560 (2011)
 - (26) Rosencher, E., & Bois, P., Model system for optical nonlinearities: Asymmetric quantum wells, *Phys. Rev. B* **44**, 11315–11327 (1991)
 - (27) Chung, I., *et al*, Helical Polymer $1/\infty$ [P2Se62-]: Strong Second Harmonic Generation Response and Phase-Change Properties of Its K and Rb Salts, *J. AM. CHEM. SOC.* **129**, 14996-15006 (2007)
 - (28) Hakuta, K., Marmet, L., & Stoicheff, B. P., Electric-field-induced second-harmonic generation with reduced absorption in atomic hydrogen, *Phys. Rev. Lett.* **66**, 596–599 (1991)

Supplemental Materials

Quantum-Enhanced Tunable Second-Order Optical Nonlinearity in Bilayer Graphene

Sanfeng Wu¹, Li Mao², Aaron M. Jones¹, Wang Yao³, Chuanwei Zhang², Xiaodong Xu^{1,4*}

¹ Department of Physics, University of Washington, Seattle, Washington 98195, USA

² Department of Physics and Astronomy, Washington State University, Pullman, Washington 99164 USA

³ Department of Physics and Center of Theoretical and Computational Physics, The University of Hong Kong, Hong Kong, China

⁴ Department of Material Science and Engineering, University of Washington, Seattle, Washington 98195, USA

*Email: xuxd@uw.edu

1. Theory for second order optical conductivity

Considering the applied potential bias between top and bottom gates, the electronic Hamiltonian near the Dirac points (\mathbf{K} and \mathbf{K}') is¹:

$$H = \sum \psi_k^\dagger \mathcal{H}_k \psi_k,$$

where

$$\psi_k^\dagger = (b_k^{1\dagger}, a_k^{1\dagger}, a_k^{2\dagger}, b_k^{2\dagger}),$$

and

$$\mathcal{H}_k = \begin{pmatrix} -\Delta & \hbar v_f g & 0 & 0 \\ \hbar v_f g^* & -\Delta & \gamma_1 & 0 \\ 0 & \gamma_1 & \Delta & \hbar v_f g \\ 0 & 0 & \hbar v_f g^* & \Delta \end{pmatrix},$$

$a_k^{i\dagger}$ ($b_k^{i\dagger}$) is the creation operator for electrons at the sublattice A (B), in the layer i ($i = 1, 2$), and with momentum \mathbf{k} in the BZ. $\mathbf{k} = (k_x, k_y)$ is the continuous wave vector from \mathbf{K}, \mathbf{K}' and $g = k_x - \xi i k_y$ is a complex number ($\xi = +1$ for \mathbf{K} and $\xi = -1$ for \mathbf{K}'). The Fermi velocity v_f is determined by the intra-layer hopping energy $\gamma_0 \approx 2.8 \text{ eV}$ between nearest neighbors. a is the lattice constant of graphene. $\gamma_1 \approx 0.4 \text{ eV}$ is the inter-layer hopping parameter between A_1 and A_2 . We ignore other hopping processes due to their relatively weak strengths. The diagonal items $\pm\Delta$ come from the potential bias between the two graphene-layers. Diagonalizing the Hamiltonian, we can obtain the energy spectrum with four branches near the Dirac point¹.

The interaction between light and BLG can be described by replacing the momentum vector $\hbar\mathbf{k}$ with¹

$$\mathbf{p} = \hbar\mathbf{k} + e\mathbf{A},$$

where $\mathbf{A} = -\mathbf{E}/(i\omega)$ is the vector potential of the incident laser beam. As an example, if the incident laser is a circularly polarized beam σ_+ , then $\mathbf{E} = \frac{E e^{i\omega t}}{2i} (1, -i) + \text{c.c.}$ The interaction between laser and electrons ($\sim 1 \text{ meV}$) is weak compared to the system energy

scale ($\sim 0.1\text{eV}$), therefore we can write the total Hamiltonian under band representation as

$$\bar{\mathcal{H}}_p = \bar{\mathcal{H}}_k + \frac{ev_f E e^{i\omega t}}{2\omega} H_\Phi.$$

where $H_\Phi = \Phi^\dagger [I \otimes (\sigma_x - i\xi\sigma_y)] \Phi$ for a circularly polarized beam σ_+ . I is a 2×2 unit matrix. $\sigma = (\sigma_x, \sigma_y)$ is the vector of Pauli matrixes. Φ is the initial eigenstate without the laser-field satisfying $\bar{\mathcal{H}}_k = \Phi^\dagger \mathcal{H}_k \Phi = \text{diag}[\epsilon_1, \epsilon_2, \epsilon_3, \epsilon_4]$, where $\epsilon_i (i = 1, 2, 3, 4)$ is the energy of the i^{th} band.

The evolution of electronic states is determined by the quantum Liouville equation^{2,3}

$$i\hbar\partial_t \rho = [\bar{\mathcal{H}}_p, \rho] - i\Gamma(\rho - \rho(t=0)),$$

where ρ is the time dependent quantum state of electrons with momentum \mathbf{k} at temperature T and chemical potential μ . Γ describes the electronic relaxation time^{4,5}. The linear and nonlinear optical response of ρ to the optical fields can be obtained by solving the Liouville equation perturbatively

$$\rho = \rho_k + [\rho_1(t)e^{i\omega t} + c.c]E + [\rho_2(t)e^{i2\omega t} + c.c]E^2 + \dots$$

The initial state $\rho_k = \text{diag}[f_1, f_2, f_3, f_4]$ is the initial state obtained from the Fermi-Dirac distribution $f_i = \frac{1}{\exp[(\epsilon_i - \mu)/k_B T] + 1}$ of electrons.

As we mentioned in the main text, the SHG does not exist unless there is an in-plane electric field. According to semi-classical electron transport theory, if there is an in-plane electric field \mathcal{E} , the Fermi surface is shifted by wavenumber $\Delta\mathbf{k} = e\tau\mathcal{E}/\hbar = m^*v_d/\hbar$ along the direction opposite the electric field owing to the negative electron charge. τ is the relaxation time, m^* is the electronic effective mass and v_d is the drift velocity. This process is responsible for the leak current $j_{sc} = \sigma_{dc}\mathcal{E}d$ measured by the ammeter, where d is the sample length perpendicular to the electric field, assuming a rectangular sample shape. Replacing v_d with the electronic mobility $u_m = |v_d/\mathcal{E}|$, we have

$$\hbar\Delta\mathbf{k} = \frac{m^*u_m j_{sc}}{\sigma_{dc}d}.$$

According to experimental data of BLG^{6,7}, we choose $m^* \approx 0.05m_e$, $u_m \approx 1 \frac{m^2}{Vs}$, $\sigma_{dc} \approx \frac{e^2}{h}$, $v_f \approx 10^6 \text{m/s}$, then $\hbar v_f \Delta\mathbf{k} \approx 0.01\text{eV}$ for a leak current $j_{sc} \approx 8 \mu\text{A}/\mu\text{m}$ (corresponding to $\mathcal{E} \approx 2000\text{V/m}$).

As a result of the shift of the Fermi surface, the initial electronic state in the presence of the in-plane applied current turns out to be

$$\rho_{\mathbf{k}} \leftarrow \rho_{\mathbf{k} - \Delta\mathbf{k}}.$$

Substituting this into the quantum Liouville equation, we obtain the first order and second order equations for the electronic-state evolution

$$\begin{aligned} i\hbar\partial_t \rho_1 - (\hbar\omega - i\Gamma)\rho_1 &= [\bar{\mathcal{H}}_k, \rho_1] + \frac{ev_f}{2\omega} [H_\Phi, \rho_k], \\ i\hbar\partial_t \rho_2 - (2\hbar\omega - i\Gamma)\rho_2 &= [\bar{\mathcal{H}}_k, \rho_2] + \frac{ev_f}{2\omega} [H_\Phi, \rho_1]. \end{aligned}$$

The dynamics of the electronic state excited by photons can be obtained by solving these two linear ordinary differential equations as a steady state problem (*i.e.*, $\partial_t \rho_1 = 0, \partial_t \rho_2 = 0$), yielding

$$\rho_1^{ij} = -\left(\frac{ev_f}{2\omega}\right) \frac{[H_\Phi, \rho_k]_{ij}}{\hbar\omega + \epsilon_{ij} - i\Gamma},$$

$$\rho_2^{ij} = -\left(\frac{ev_f}{2\omega}\right) \frac{[H_\Phi, \rho_1]_{ij}}{2\hbar\omega + \epsilon_{ij} - i\Gamma}.$$

The induced electric current is defined as

$$j_e = ve \sum_{BZ} \text{tr}(\rho \frac{\partial \mathcal{H}_p}{\partial \mathbf{p}}) = \sigma_1 E e^{i\omega t} + \sigma_2 E^2 e^{i2\omega t} + c.c + \dots.$$

where $v = 2$ describes the spin degeneracy and σ_1 is the linear optical conductivity. We have confirmed that our result for σ_1 is exactly the same as that in former literature on BLG using the Kubo formula. Here we focus on the second order nonlinear optical conductivity σ_2 , which stimulates SHG. The result is

$$\sigma_2^\alpha = 2e \sum_{BZ} \text{tr} \left(\rho_2 \frac{\partial \mathcal{H}_p}{\partial p_\alpha} \right) = 2ev_f \sum_{K, K'} \text{tr}(\rho_2 \eta_\Phi^\alpha)$$

$$= \frac{e^3 v_f^2}{8\pi^2 \omega^2} \int_{BZ} \sum_{ijl} \left[\frac{\rho_k^{ii} - \rho_k^{ll}}{\hbar\omega + \epsilon_i - \epsilon_l - i\Gamma} - \frac{\rho_k^{ll} - \rho_k^{jj}}{\hbar\omega + \epsilon_l - \epsilon_j - i\Gamma} \right] \frac{(H_\Phi)_{il} (H_\Phi)_{lj} (\eta_\Phi^\alpha)_{ji}}{2\hbar\omega + \epsilon_i - \epsilon_j - i\Gamma} d\mathbf{k}.$$

Here $\eta_\Phi^\alpha = \frac{\partial \mathcal{H}_p}{\partial p_\alpha} = v_f \Phi^\dagger (I \otimes \sigma_\alpha) \Phi$ for Dirac cone K and $\eta_\Phi^\alpha = v_f \Phi^\dagger (I \otimes \sigma_\alpha^*) \Phi$ for K'. $i, j, l = 1, 2, 3, 4$ and the integration over k is performed in the vicinity of K or K'. $\alpha = x, y$ represents the axis direction in the graphene plane.

2. Effects of Γ

We set $\Gamma = 0.05\text{eV}$ in our calculation in the main text. The value of Γ affects the magnitude of the second order optical conductivity significantly. In Fig. 1S, we show σ_2 as a function of Γ and the incident laser frequency ω . The incident laser is polarized along the x direction and $T=30\text{K}$. Apparently, the signal intensity becomes larger when the relaxation time of the excited electronic state becomes longer, i.e., smaller Γ .

3. Effects of the direction of the in-plane DC current

To achieve SHG, we have to apply an in-plane electric field. In the main text, we apply an in-plane current along the y direction as an example. In general, the direction of the field is not unique. One can obtain giant optical nonlinear conductivity by inducing a current in any direction in the 2D atomic plane. This is important in practice because the in-plane current may not lie in the y direction defined by the atomic structure (See Fig. 1 in the main text). Here we show the results for a different direction ($-y'$) of the in-plane current with a linearly polarized incident laser at $T=30\text{K}$ (See Fig. 2S). We show that it is the direction of the DC current that determines the symmetric axis for second order optical conductivity (Fig. 2S c and d).

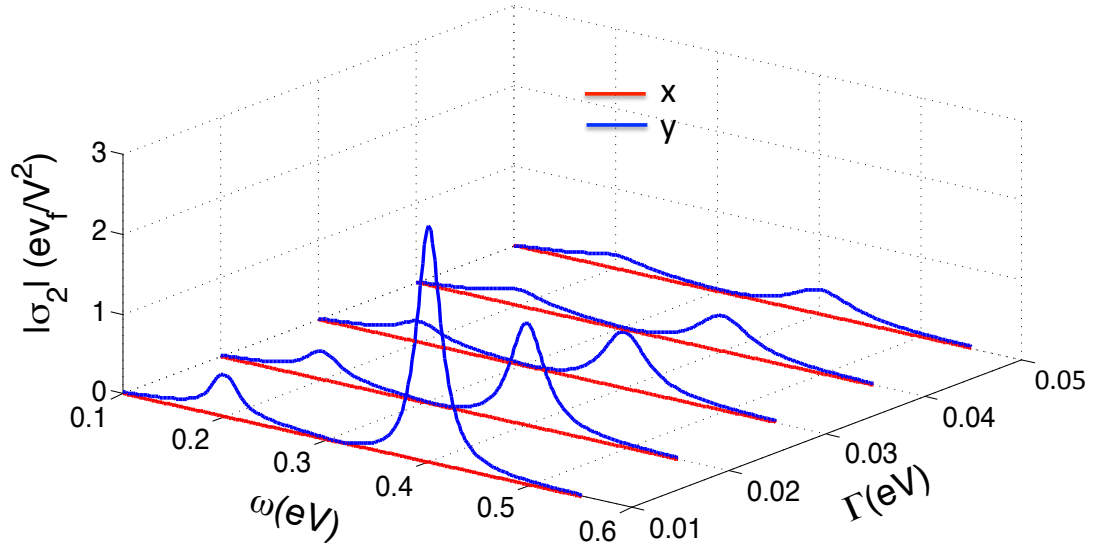


Figure 1S | Effects of relaxation time of excited states on SHG. The incident laser is linearly polarized and $T=30$ K. Blue line denotes the second order optical conductivity in the y direction and red in the x direction.

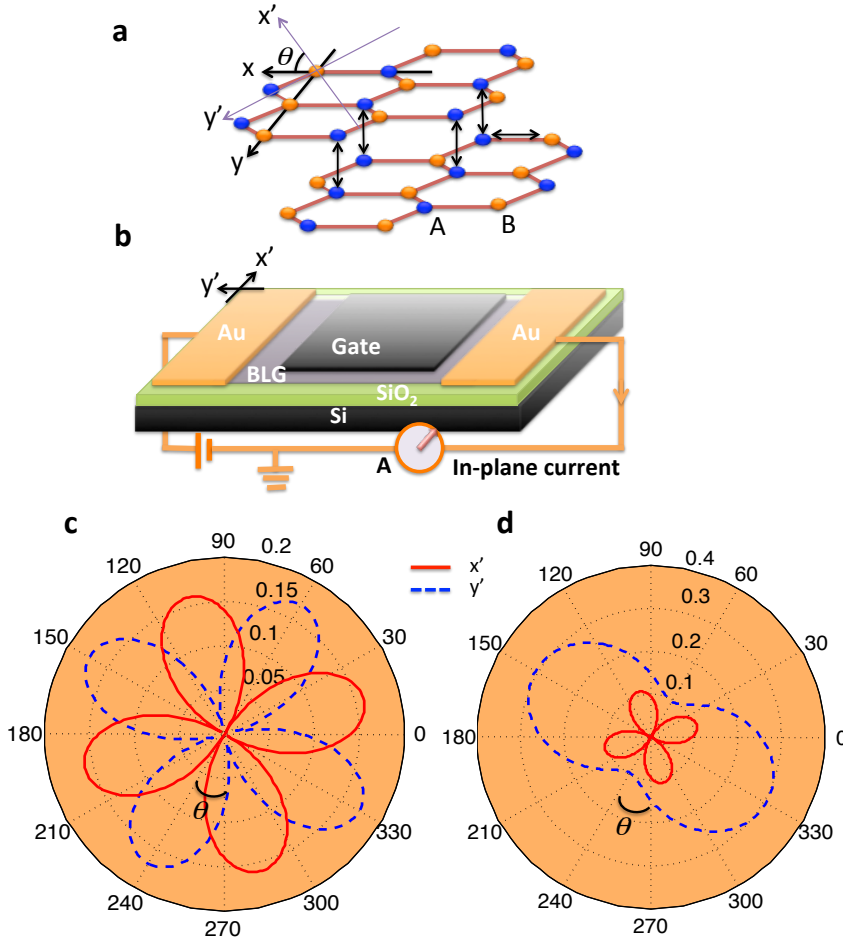


Figure 2S | Effect of the direction of in-plane electric field on SHG. **a**, Atomic structure of BLG. (x, y) and the coordinates used for tight-binding model. $(-y')$ is the direction of the DC current as shown in **b**. **b**, Normal device scheme of BLG, which determines the direction of the current, which is usually not along the axis of the coordinates (x, y) in **a**. The deviation is described by an angle θ . **c** and **d**, polar plots of the intensity of the second order optical conductivity in the x' and y' direction at $T=30$ K for incident laser frequency (**c**) $\omega = 0.2$ eV and (**d**) $\omega = 0.4$ eV. We can see that the direction of the in-plane field determines the symmetric axis (shown by θ) of the optical nonlinearity. Polar angle is the polarization angle of the incident beam starting from the x -axis.

Reference:

- (1) Neto, A. H. C., *et al.*, The electronic properties of graphene, *Rev. Mod. Phys.* **81**, 109 (2009).
- (2) Hendry, E., *et al.*, Coherent Nonlinear Optical Response of Graphene, *Phys. Rev. Lett.* **105**, 097401 (2010)
- (3) Landau, L. D., & Lifshitz, E. M. (1977). Quantum Mechanics, Non-Relativistic Theory: Volume 3. Oxford: Pergamon Press. pp. 41. ISBN 0080178014.; Sakurai, J.J., Modern Quantum Mechanics, revised edition, by Addison-Wesley Publishing Company, Inc. 1994
- (4) Nandkishore, R., & Levitov, L., Polar Kerr Effect and Time Reversal Symmetry Breaking in Bilayer Graphene, *Phys. Rev. Lett.* **107**, 097402 (2011)
- (5) Yang, H., Feng, X., Wang, Q., Huang, H., Wei Chen, W., Wee, A. T. S., & Ji, W., Giant Two-Photon Absorption in Bilayer Graphene, *Nano Lett.*, **11** (7), pp 2622–2627, (2011).
- (6) Zhang L. M., *et al.*, Determination of the electronic structure of bilayer graphene from infrared spectroscopy, *Phys. Rev. B* **78**, 235408 (2008)
- (7) Zou K., *et al.*, Effective mass of electrons and holes in bilayer graphene: Electron-hole asymmetry and electron-electron interaction, *Phys. Rev. B* **84**, 085408 (2011)